A REVIEW OF ACTIVE CONTROL APPLIED TO PLATES AND CYLINDERS

Nicole Kessissoglou
School of Mechanical and Manufacturing Engineering
The University of New South Wales, Sydney, 2052

This paper presents adaptive feedforward active control applied to simple structures comprised of beam, plate and cylindrical elements. For each system under consideration, by initially obtaining a good understanding of the physics of the structural and acoustic responses, the active control application can be tuned to improve the control performance. In particular, the use of active structural acoustic control to attenuate the structurally radiated sound fields is investigated.

INTRODUCTION

Sound radiation from distributed vibrating structures is a continuous problem in transportation and other industries. At low frequencies, passive control techniques provide a poor reduction in structural dynamic responses, promoting active control as a more attractive solution. A novel approach to actively attenuate the structurally radiated sound fields is to directly modify the structural response. This is achieved by adding control inputs to the structure. The acoustic cost function is typically based on a global measure such as the radiated sound power, or the local sound pressure. This control technique is known as active structural acoustic control (ASAC).

Previous work on active control of sound radiating from structures has mainly dealt with homogeneous structures such as beams (Burdisso and Fuller, 1992) and plates (Fuller *et al.*, 1991; Wang *et al.*, 1991; Pan *et al.*, 1992). Using actuator and sensor mechanisms associated with smart structures, ASAC strategies have been applied utilising piezoelectric materials as both the structural actuator and error sensor (Clark and Fuller, 1992). In this ASAC strategy, where the structure is equipped with a sensor bonded to the surface, can be practical in cases when the use of acoustic sources such as microphones or hydrophones located in the surrounding fluid may not be practical (for example, in the case to actively suppress the externally radiated sound field from a submarine). It is important to note however that when using structural error sensors in an ASAC application, it is necessary to have an efficient design procedure and good *a priori* knowledge of the structure-acoustic coupling, due to the inability of the structural sensors to directly measure the acoustic response.

ASAC techniques have also been employed to attenuate the structure-borne sound fields generated from subsonic wave scattering at a structural discontinuity, which may be a boundary (Guigou and Fuller, 1993), a line discontinuity (Gu and Fuller, 1991) or a beam-stiffened plate (Kessissoglou and Pan, 1998). In these cases, it has been shown that whilst the influence of flexural near-field waves generated due to the presence of a structural discontinuity can be neglected in terms of the dynamic response, they significantly contribute to the far-field structurally radiated sound.

While most ASAC systems are designed using feedforward control techniques, active control of the radiated sound pressure from a simply supported plate has been investigated using feedback control (Meirovitch and Thangjitham, 1990). A good review of ASAC applied to plate systems and cylindrical structures is given by Fuller *et al.* (1996). This paper reviews the use of active vibration control (AVC) and active structural acoustic control (ASAC) based on a conventional adaptive feedforward algorithm, to respectively attenuate the structural and acoustic responses associated with a beam-stiffened plate and a cylinder submerged in a fluid.

OVERVIEW OF ADAPTIVE FEEDFORWARD ACTIVE CONTROL

The objective of feedforward control is to produce a secondary disturbance to a system that cancels the effect of a primary disturbance at the location of an error sensor. Adaptive feedforward active control is effective in situations of tonal noise and when a reference signal correlated to the primary disturbance is available. This signal is passed through an adaptive filter, as shown in Fig. 1, where the output of the adaptive filter is applied to the physical system by secondary sources. The filter coefficients are adapted in such a way that the error signal at one or more critical points is minimised.
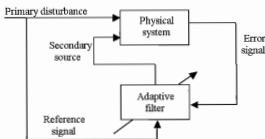

Figure 1. Block diagram of an adaptive feedforward control system (Widrow and Stearns, 1985).

Local control is achieved as there is no guarantee that the response is reduced at other locations other than the error sensor. Unless the response is dominated by a single mode, there are locations where the total response may be

amplified. Using the conventional adaptive feedforward least mean square (LMS) algorithm (Fuller *et al.*, 1996), the optimal control force is obtained in what follows. Let the primary structural response (such as the flexural displacement of a beam or plate) be denoted by $w_p(\mathbf{x})$. This can often be written in terms of the product of the system transfer function G_p and the primary disturbing force F_p, that is, $w_p(\mathbf{x})=F_p G_p(\mathbf{x})$. When a control point force of amplitude F_s applied at a position $\mathbf{x}_s$ on the system, the secondary structural response can be expressed as $w_s(\mathbf{x})=F_s G_s(\mathbf{x})$, where G_s is the secondary transfer function. The total response at some point $\mathbf{x}$ can be obtained by adding the structural responses induced by the primary disturbance and the control force:

$$w_{tot}(\mathbf{x}) = w_p(\mathbf{x}) + w_s(\mathbf{x}) \qquad (1)$$

A variety of cost functions can be developed depending on the response to be minimised; these cost functions may be the squared displacement or acceleration, kinetic energy, transmitted power, mean square sound pressure, out-of-plane velocity, etc. Using the squared error sensor output at a location $\mathbf{x}_e$ as the cost function to be minimised, a quadratic function expression in terms of the complex control force amplitude is obtained as:

$$J = w_{tot}(w_{tot})^* = F_s^* A F_s + F_s^* B + F_s B^* + C \qquad (2)$$

where the asterisk '*' denotes the complex conjugate, and $A = G_s^* G_s$, $B = G_s^* G_p F_p$ and $C = F_p^* G_p^* G_p F_p$. In the adaptive feedforward LMS algorithm, the optimal control force that results in the minimisation of the cost function can be obtained by differentiating the cost function with respect to the real and imaginary components of the control force (Fuller *et al.*, 1996). The optimal control force corresponds to the force value when both derivatives are zero, that is $(\partial J/\partial F_{s,\text{real}})=0$ and $(\partial J/\partial F_{s,\text{imag}})=0$. The optimal control force can then be obtained as:

$$F_{s,opt} = F_{s,\text{real}} + jF_{s,\text{imag}} = -\frac{B}{A}. \qquad (3)$$

APPLICATIONS OF AVC AND ASAC

AVC of the wave transmission in a rib-stiffened plate

Beam stiffened plates are commonly found in ship hulls, aircraft and machine casing. The transmission of plate flexural waves through a reinforcing beam is related to the coupling between the plate flexural waves and the flexural and torsional waves in the beam. For an infinite beam-stiffened plate, the maximum flexural wave transmission occurs at the optimal trace wave matching between the flexural waves in the plate and the flexural and torsional waves in the beam. These are described as flexural and torsional wave *coincidence* conditions, respectively. The coincidence conditions are dependent on the angle of incidence φ of the flexural plane wave W_{in} propagating in the x-y plane in plate 1 and impinging on the beam boundary, as shown in Fig. 2.

The relationship between the wavenumber k and the wavelength λ ($k=2\pi/\lambda$) allows the explanation of the coincidence conditions. The plane wave in plate 1 at a frequency ω has wavelength λ_p, while the wavelength of the
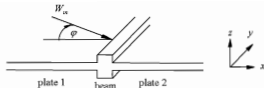

Figure 2. Beam-stiffened plate separated into three subsystems: plate 1, beam and plate 2, showing the flexural plane wave in plate 1 incident at the beam boundary.

flexural wave in the beam at frequency ω is λ_f. λ_x and λ_g are not necessarily equal. If the intercepts of the incident wave on the y-axis equals the natural flexural wavelength of the beam as shown in Fig. 3, then optimal flexural trace wave matching occurs (flexural coincidence). Similarly, if λ_y matches the natural torsional wavelength of the beam ($\lambda_y = \lambda_g / \sin \varphi = \lambda_t$), then optimal trace wave matching occurs between the plate flexural waves and the beam torsional waves (torsional coincidence). It is at these coincidence conditions that greatest coupling between the plate and beam motion occurs, resulting in the maximum transmission of the flexural wave motion through the reinforcing beam. Since the plate and beam flexural wavenumbers vary with frequency in the same way, the flexural coincidence condition becomes frequency independent and occurs for a single angle of incidence only ($\varphi = \sin^{-1}(k_p/k_f)$). The torsional coincidence condition is dependent on both angle and frequency, that is, the angle at which this coincidence condition occurs increases with the corresponding coincidence frequency ($\varphi = \sin^{-1}(k_p/k_t)$).

The characteristics of the transmission of the plate flexural waves through the reinforcing beam are shown in Fig. 4 for a frequency range up to 2000 Hz and for a relevant range of angles of the incident waves from 0° to 20°. The beam-stiffened plate has material properties of aluminium, with a structural loss factor of 0.001, plate thickness of 1.6 mm, and beams of both width and height of 20mm. The size of the beams has been chosen to greatly exaggerate the coincidence conditions. Figure 4 shows that the flexural coincidence condition occurs for a single incident angle corresponding to $\varphi_p = 11.5°$ for this beam-plate model. At torsional coincidence, the angle of incidence increases with frequency.

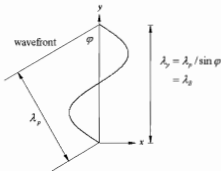Figure 3. Optimal trace wave matching between the plate and beam flexural waves
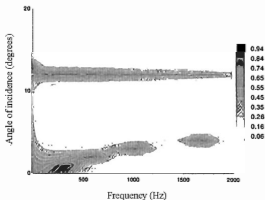
$$\lambda_y = \lambda_g / \sin \varphi = \lambda_g$$

Figure 4. Flexural wave transmission in plate 2 showing flexural and torsional coincidences.

An array of point control forces are applied along the length of the beam to excite flexural motion, and are equally distributed by a distance Δ (Kessissoglou & Pan, 1997). Similarly, point control moments can be applied to excite torsional motion in the beam. The error sensors are located in the far field of plate 2. Under plane wave propagation, the control forces are arranged to have the same magnitudes and prefixed phases as follows:

$$F_n^s = F_s e^{i\phi_n}, \quad n = -N,...,N \quad (4)$$

For attenuation of the flexural wave transmission due to flexural coincidence, the phases of the control forces can be arranged to have the same spatial phase variation to that of the primary flexural waves in the beam. The phases of the control forces become:

$$\phi_n = k_B n\Delta, \quad n = -N,...,N \quad (5)$$

where $\Delta=0.3\lambda_B$. It should be noted that this arrangement is similar to the biologically inspired control strategy, where a group of actuators are connected together with certain phase and amplitude relationship, and only one control signal is needed to drive them (Carneal and Fuller, 1995). Under point moment control, the phases of the control moments are arranged to be $\phi_n=k_T n\Delta$ where $\Delta=0.5\lambda_T$. The displacement at the error sensor locations in the far-field of plate 2 is the superposition of the primary transmitted waves and secondary flexural waves generated by the control forces. The cost function to be minimised is the squared total plate flexural displacement at the error sensor location $x_s=10\lambda_p$ and averaged at M discrete locations along the y-direction.

Figure 5 shows the flexural wave attenuation level at the error sensor locations ($x_s=10\lambda_p$) and for 401 discrete locations along the y-direction corresponding to the range ($-2\lambda_p,2\lambda_p$). Examination of a relevant range for the incident angle from 0° to 20° at excitation frequencies of 500 Hz and 1000 Hz shows that significant attenuation of around 14 dB has been achieved at the flexural coincidence angle of $\varphi_p\approx11.5°$. The level of attenuation at both frequencies is the same. Due to the nature of the arranged control force excitation, the radiated secondary
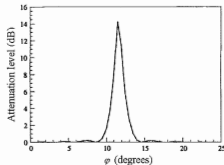

Figure 5. Attenuation levels of the flexural wave transmission at excitation frequencies of 500 Hz (solid line) and 1000 Hz (dashed line) using point control forces.
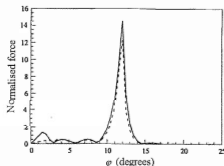

Figure 6. Normalised magnitude of the optimal control force at 500 Hz (solid line) and 1000 Hz (dashed line).
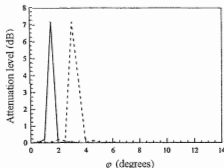

Figure 7. Attenuation levels of the flexural wave transmission at excitation frequencies of 500 Hz (solid line) and 1000 Hz (dashed line) using point control moments.

flexural waves have poor spatial phase correlation with the transmitted primary waves away from the flexural coincidence angle, which results in poor attenuation. However, away from the coincidence condition, the beam itself acts as an effective passive attenuation device. Changing the frequency of excitation has no effect on the attenuation level or the angle at which attenuation is achieved, as the flexural coincidence condition is independent of frequency.
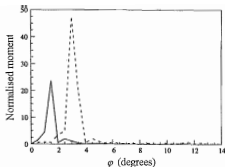
Figure 8. Normalised magnitudes of the optimal control moments at 500 Hz (solid line) and 1000 Hz (dashed line).

Figure 6 shows the corresponding dimensionless magnitude of the optimal control force $F_{c,opt}$, which shows that a large force is required at the flexural coincidence angle. As the frequency increases, the beam is able to vibrate more freely and hence a slightly smaller amplitude of the control forces is required in order to generate secondary vibrational levels in the beam to match the primary flexural energy level in the beam.

Under point moment control, attenuation of the flexural wave transmission is achieved for the same number of discrete locations along the y-direction as for the point control force application, corresponding to the range $(-2\lambda_p:2\lambda_p)$. Figure 7 shows the attenuation levels of the flexural wave transmission using point control moments at excitation frequencies of 500 Hz and 1000 Hz. The peaks of the attenuation levels occur at the corresponding torsional coincidence angles of 1.5° and 3°, respectively. Unlike force control, as the frequency increases, the magnitudes of the control moments required for the same level of attenuation increases (Fig. 8). This is due to the fact that at higher frequencies, the beam torsional stiffness relative to the plate bending stiffness increases (Goyder and White, 1980).

ASAC of a rib-stiffened plate

Using ASAC, the dynamic response of the ribbed plate can be modified to attenuate the structurally radiated sound field. In this ASAC application, the control forces are again applied to the beam, while the error sensing devices are located in the surrounding fluid. An incident wave propagating in the low frequency range corresponding to frequencies well below critical (where the *in vacuo* speed of the flexural waves in the plate c_b is less than the speed of sound in the fluid c_0), is known as a subsonic wave and does not radiate energy into the far-field of the surrounding fluid. When the subsonic flexural wave is incident on the beam discontinuity, the scattering of the structural wave field generates both supersonic and subsonic wave types in the structural response, resulting in structurally radiated sound. The structure is considered to be in air and hence the response is not affected by the fluid loading. For periodic distribution of the sound pressure in the y-direction (along the length of the beam), the sound pressure field is evaluated in a cylindrical coordinate system defined by $x=r\cos\theta$, $z=r\sin\theta$, $y=0$, as shown in Fig. 9.
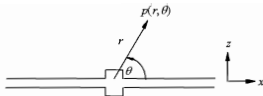

Figure 9. Sound pressure field evaluated in a cylindrical co-ordinate system in the x-z plane.

An expression for the sound pressure field of the ribbed plate under plane wave incidence has been derived using the acoustic wave equation and structure-fluid coupling conditions at the surface of the plate (Junger and Feit, 1985). The expression for the primary sound pressure field is described in terms of both a non-integral component and an integration of the structural wavenumber spectrum. Each component is a function of the scattered structural waves (transmitted and reflected, propagating and evanescent plate flexural waves). The wavenumber spectrum of the integral component can be separated into supersonic and subsonic wavenumber spectrums. The supersonic wavenumber spectrum directly contributes to the far-field radiating sound pressure, whereas the subsonic wavenumber spectrum dominates the near-field acoustic response. The supersonic wavenumber spectrum is further restricted by a limiting range for the incident angle, where φ must be less than the critical incident angle φ_c, which is defined by $\varphi_c=\sin^{-1}(k_a/k_b)$ and k_a is the acoustic wavenumber ($k_a=\omega/c_0$).

The primary radiated sound power is obtained by integrating the acoustic intensity over a semi-cylindrical surface centred at the beam discontinuity, where the acoustic intensity is related to the mean square pressure. At the structural coincidence conditions, the far-field primary sound pressure level is slightly decreased. This is due to the fact that at the coincidences, there is a large amount of flexural wave transmission through the reinforcing beam, thereby resulting in a more balanced distribution of the structural waves along the x-direction (normal to the beam). It has been previously shown that an imbalance in the structural wavenumber along the x-direction will generate a greater number of supersonic wavenumber components, which will thereby result in an increase in the far-field radiated sound pressure. The phases of the control forces are pre-fixed such that the forces have a spatial phase variation with each other at the flexural coincidence condition. Although the primary structural response may be either at coincidence or off-coincidence, the secondary structural response is always generated by forces with the phase delay in the beam corresponding to that of the flexural coincidence condition. At flexural coincidence, the total-far-field sound pressure due to the superposition of the primary and secondary sound fields is optimised. At any off-coincidence condition, the superposition of the primary and secondary sound fields will result in the least increase in the supersonic wavenumber components to be attenuated.

Using the control force approach described previously, in which for $2N+1$ forces applied to the beam, the control

forces have a pre-fixed phase relationship with each, only the complex amplitude F_s needs to be optimised. For minimisation of the acoustic responses, two cost functions are examined corresponding to (i) the square of the total sound pressure $|p_{tot}(r,\theta)|^2$ at a far-field control location (r_c,θ_c), and (ii) the radiated sound power. An expression for the total sound pressure is obtained by the superposition of the primary and secondary sound fields (Kessissoglou and Pan, 1998). Both cost functions can be expressed as a quadratic function in terms of the control force amplitude. Using the adaptive feedforward LMS algorithm, the optimal control force is obtained.

Using the same material properties and dimensions of the ribbed plate and to represent the surrounding acoustic field, the flexural and torsional coincidence angles are respectively $\varphi_b=11.5°$ and $\varphi_t=1.5°$ (for an excitation frequency of 500Hz). The critical incident angle defined by $\varphi_c=\sin^{-1}(k_a/k_o)$ is 14.5°. Since both coincidence angles are less than critical, they both contribute to the radiation of sound into the far-field. Figure 10 shows that only those incident waves with angles less than the critical incident angle contribute to the radiated sound power, as these angles correspond to the supersonic wavenumber spectrum (Kessissoglou and Pan, 1998). At incident angles greater than critical, there is very little sound power radiated into the far-field as the sound power is dominated by the subsonic wavenumber spectrum which only contributes to the acoustic near-field. An interesting feature in Fig. 10 is the effect of the structural coincidences on the far-field radiated sound power. At the structural coincidence conditions corresponding to $\varphi=1.5°$ and $11.5°$, there is a decrease in the radiated sound power. This due to the fact that at a structural coincidence condition, the greatest plate flexural wave transmission through the beam occurs. As a result, the structural energy is more uniformly distributed in the plate and less energy is radiated into the acoustic fluid. As the incident angle approaches critical, the far-field sound power is a maximum as this condition corresponds to the optimal coupling between the structure and the fluid.
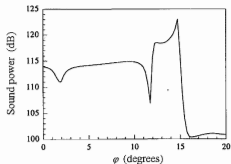
Figure 10. Radiated sound power as a function of the angles of the incident wave.

The radiated primary sound pressure at a far-field dimensionless radius of $k_a r=10$ increases at directivity angles close to the surface of the plate ($0°\leq\theta\leq5°$ and $175°\leq\theta\leq180°$). This is due to the fact that even at a far-field radius, directivity

angles close to the surface of the plate correspond to the near-field. Therefore, in order to accurately represent the radiated sound power, these 'grazing' angles were not included in the integration of the sound intensity, that is, the sound power was evaluated over the hemispherical range of $5°\leq\theta\leq175°$ (centred on the beam).

Figure 11 presents the attenuated sound power as a function of the error sensor location θ_e for an incident angle of $11.5°$ (flexural coincidence). The attenuated sound power resulting from minimisation of the sound power and from minimisation of the far-field sound pressure at each local error sensor location in the range of $5°\leq\theta\leq175°$ are compared. For the present control arrangement, using the radiated sound power as the cost function results in attenuation levels of 23dB, 16dB and 36dB for incident angles of $5°$ (off coincidence), $11.5°$ (flexural coincidence) and $14.5°$ (critical angle), respectively. Similar levels of sound power attenuation can be achieved by minimising the local sound pressure using a single error sensor located in the range of $45°\leq\theta_e\leq50°$ or $130°\leq\theta_e\leq135°$. The exact location for the optimal error sensor differs slightly for each incident angle of the incoming structural wave. Examination of the controlled sound pressure levels show that optimising the error sensor location results in a reduction in the radiation efficiency. The ASAC system can now be designed with an appropriate cost function and error sensor location to achieve the best control performance. For a single, optimally located error sensor, it has been shown that global attenuation of the squared pressure is achieved at all directivity angles away from the grazing angles (Kessissoglou and Pan, 1998). This reduces the complexity of the control application since using the sound power as the cost function would require an array of error sensors located in a hemisphere centred on the ribbed plate.
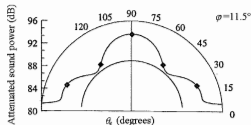
Figure 11. Attenuated sound power as a function of the local error sensor location θ_e, resulting from minimisation of the sound power (solid line) and from minimisation of the far-field sound pressure at each local error sensor location in the range of $5°\leq\theta_e\leq175$.

Active control of a finite cylinder

Active control of the structural and acoustic responses of cylinders has mainly concentrated on actuating and minimising the radial motion of the cylindrical shell. A review of earlier literature on active control to minimize cylinder interior acoustic fields (in the case of an aircraft interior) and exterior acoustic fields (in the case of sound radiation from a submarine or noise from piping systems) is given by Fuller et al. (1996). Active control of sound radiation from cylinders

using piezoelectric actuators and structural sensors has shown to yield similar performances in attenuating the far-field radiated pressure as error microphones (Maillard and Fuller, 1999). In this section it is demonstrated that active modal control of both the axial and radial motions of a finite cylinder is required to globally attenuate the structurally radiated sound pressure. An idealized model of a submarine hull is considered, which is modelled as a ring-stiffened cylindrical shell with finite rigid end closures, separated by bulkheads into a number of compartments and under axial excitation from the propeller-shafting system (Tso *et al.*, 2003; Dylejko *et al.*, 2005). The fluid loading effects are modelled as an increase in inertia of the shell. Lumped masses are added at each end to represent on-board equipment and to maintain a condition of neutral buoyancy. A schematic of the submarine model is shown in Fig. 12. Excitation of the hull axial modes causes both axial motion of the end closures, u, and radial motion of the shell, w, resulting in a high level of structurally radiated noise. Under axial excitation, it is assumed that only the breathing mode of the cylinder is excited which gives rise to an axisymmetric case. An expression for the radiated sound pressure contributed by axial movement of the end plates and radial motion of the shell was obtained using the Helmholtz integral equation (Junger and Feit, 1985), and by considering the radiating surfaces separately.
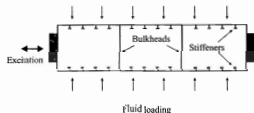
Figure 12. Schematic of the hull under axial excitation.

A secondary axial force F_y was used to excite the pressure hull at $x=L$, as shown in Fig. 13. For active control of the axial response of the end closures, an error sensor was located at each end of the pressure hull, denoted by $es*$. For control of the radial response of the hull, one or more rings of error sensors, $es*$, were located circumferentially around the hull. It is important to note that due to the Poisson effect which causes coupling between the axial and radial motions of the hull, the use of a control force to generate a secondary axial response will also generate secondary radial motion. Similarly, active control of the radial motion will also result in secondary axial vibration. This must be taken into account in the evaluation of the total radiating sound pressure due to the primary and control forces. The squared total axial and radial displacements due to the primary and control excitations were minimised at the error sensors using the adaptive feedforward LMS algorithm described previously. When both the axial and radial displacements were simultaneously controlled, two control forces were used, one for each of the displacements.

Numerical calculations were performed on a ring stiffened steel cylinder of 6.5 m diameter, 40 mm hull plate thickness, 45 m length, and with two evenly spaced bulkheads of thickness
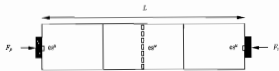
40 mm. The cylinder was submerged in water of density 1000 kg/m³. A neutrally buoyant condition was maintained by using a distributed mass of 1000 kg/m³, and with lumped masses of 200 tonnes at each end. Internal structural damping was included in the analysis by using a structural loss factor of 0.02. A primary axial force of 1 N is applied to one end of the hull. The first three axial resonances were observed to be approximately 20.5, 42 and 64 Hz, as shown in figure 14. The small peak at approximately 54 Hz is caused by the resonance of the bulkheads. At the first and third resonances, the end plates of the cylinder are vibrating out of phase with each other. At the second axial mode, when the plates of the cylinder are vibrating in phase, the axial response of the end plates accounts for approximately two-thirds of the primary radiated pressure.
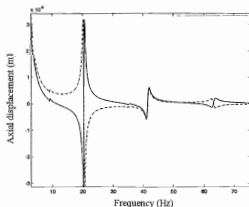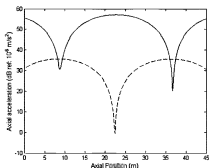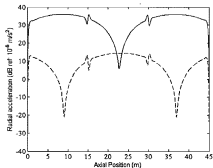
Figure 14. Axial response of the hull at $x=0$ (solid line) and $x=L$ (dashed line).

Active vibration control was applied at the second axial resonance of 42 Hz. Figures 15(a) and (b) present the primary and controlled responses of the axial and radial motions, respectively, as a function of axial position along the hull (from $x=0$ to L). Comparison of the primary axial and radial motions shows that when the axial response is a maximum (at the cylinder ends and midway along the hull length for the second axial mode), the radial response is a minimum, and vice versa. Figure 15(b) also shows the localised effect of the bulkheads. In Fig. 15(a), the squared axial displacement was simultaneously minimised at each end of the pressure hull. In Fig. 15(b), the squared radial

Figure 13. Locations of the control force and error sensors for active control of the axial and radial motions of the finite hull.

Figure 15. Primary (solid line) and controlled (dashed line) acceleration distributions of the axial (a) and radial (b) responses as a function of axial position along the length of the hull.

displacement was simultaneously minimised at two rings of error sensors located at anti-nodal axial positions along the hull length. The corresponding magnitudes of the control forces are nearly unity, attributed to the axisymmetric motion of the hull and symmetry of the control application.
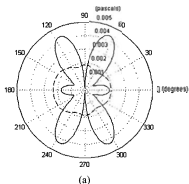
Figure 16 shows the primary structurally radiated sound pressure for control of the radial response only and for control of both the axial and radial responses is given in Figs. 16(a) and (b), respectively. For control of the radial response, the control performance is strongly dependent on the error sensor locations for a given axial resonant frequency. Active control of both the axial and radial hull displacements results in complete cancellation of the radiated sound pressure.

Excitation of the hull at one of its low frequency axial resonant frequencies results in an efficiently radiating structural mode. Due to the coupling between the axial and radial motions of the cylinder, a control actuator for each wave type is required. However, due to active control at a resonant frequency, the use of a single actuator for each wave type is sufficient. For active control at an off-resonant frequency, the modal density is higher and an increase in the number of control actuators is required to improve the control

performance. The number of error sensors should either be equal or greater than the number of control inputs used. Increase the number of error sensors can generally improve the attenuation achieved due to the cost function being closer to an estimate of a global property (such as kinetic energy or sound power), and is thereby much more robust to changes in the physical system response.

CONCLUSIONS

This paper presents a review of adaptive feedforward active control and its applications to attenuate the structural and acoustic responses associated with beam-stiffened plate and cylindrical structures. In each case, *a priori* knowledge of the dynamics of the physical system has enabled arrangement of the control actuators and sensors to improve the control performance. For active control of the flexural wave transmission through the reinforcing beam of a stiffened plate, global attenuation of the plate vibration can be achieved using an array of point forces or moments to the beam. Mechanisms of the global control are due to the significant reduction in the beam flexural or torsional energy using an array of control forces or moments, respectively. The control arrangement is
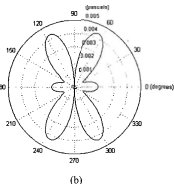
Figure 16. Primary (solid line) and controlled (dashed line) radiated sound pressure for active control of the radial response only (a) and both the axial and radial responses (b).

dependent on a pre-fixed phase relationship between the forces or moments using information on the flexural or torsional coincidences. Global attenuation of the structurally radiated sound fields can be achieved by carefully selecting the location of a single acoustic error sensor. In the case of a finite cylinder with rigid end caps excited at an axial resonance, active control of both the axial and radial motions is required to globally attenuate its acoustic signature. It is important to note that the arrangement of the control actuators and error sensors in the cases presented in this paper and corresponding levels of attenuation achieved, are dependent on coincidence or resonance conditions, at which the angles of the incident structural waves or modes of vibration contributing to the structural and acoustic responses are clearly defined.

ACKNOWLEDGEMENTS

REFERENCES

1. R.A. Burdisso and C.R. Fuller, "Dynamic behaviour of structural-acoustic systems in feedforward control of sound radiation", *J. Acoust. Soc. Am.* **92**, 277-286 (1992).
2. J.P. Carneal and C.R. Fuller, "A biologically inspired controller", *J. Acoust. Soc. Am.* **98**, 386-396 (1995).
3. R.L. Clark and C.R. Fuller, "Experiments on active control of structurally radiated sound using multiple piezoceramic actuators", *J. Acoust. Soc. Am.* **91**, 3313-3320 (1992).
4. P.G. Dylejko, N.J. Kessissoglou, Y.K. Tso and C.J. Norwood, "Reduction of the acoustic signature of a submerged vessel", *Proc. Acoustics 2005*, 9-11 November 2005, Busselton, Western Australia, pp. 427-432.
5. C.R. Fuller, S.J. Elliott and P.A. Nelson, *Active control of vibration*, London, Academic Press, 1996.
6. C.R. Fuller, C.H. Hansen and S.D. Snyder, "Experiments on active control of sound radiation from a panel using a piezoceramic actuator", *J. Sound Vib.* **150**, 179-190 (1991).
7. H.G.D. Goyder and R.G. White, "Vibrational power flow from machines into built-up structures, Part II: Wave propagation and power flow in beam-stiffened plates", *J. Sound Vib.* **68**, 77-96 (1980).
8. Y. Gu and C.R. Fuller, "Active control of sound radiation due to subsonic wave scattering from discontinuities on fluid-loaded plates. I: far-field pressure", *J. Acoust. Soc. Am.* **90**, 2020-2026 (1991).
9. C. Guigou and C.R. Fuller, "Active control of sound radiation from a semi-infinite elastic beam with a clamped edge", *J. Sound Vib.* **168**, 507-523 (1993).
10. M.C. Junger and D. Feit, *Sound, structures and their interaction*, MIT Press, 1985.
11. N.J. Kessissoglou and J. Pan, "An analytical investigation of the active attenuation of the plate flexural wave transmission through a reinforcing beam", *J. Acoust. Soc. Am.* **102**, 3530-3541 (1997).
12. N.J. Kessissoglou and J. Pan, "Active structural acoustic control of an infinite ribbed plate under light fluid-loading", *J. Acoust. Soc. Am.* **104**, 3398-3407 (1998).
13. N.J. Kessissoglou and J. Pan, "The effect of the structural coincidences on the acoustic fields radiating from a ribbed plate", *Int. J. Acoustics Vib.* **5**, 15-22 (2000).
14. J.P. Maillard and C.R. Fuller, "Active control of sound radiation from cylinders with piezoelectric actuators and structural acoustic sensing", *J. Sound Vib.* **222**, 363-388 (1999).
15. L. Meirovitch and S. Thangjitham, "Active control of sound radiation pressure", *ASME J. Vib. Acoust.* **112**, 237-244 (1990).
16. J. Pan, S.D. Snyder, C.H. Hansen and C.R. Fuller, "Active control of far-field sound radiation by a rectangular panel - A general analysis", *J. Acoust. Soc. Am.* **91**, 2056-2066 (1992).
17. Y. Tso, N.J. Kessissoglou, and C. Norwood, "Active control of a fluid-loaded cylindrical shell, part 1: dynamics of the physical system", *Proc. Eighth Western Pacific Acoust Conf (Wespac-8)*, Melbourne, Australia, 7-9 April 2003, Paper WE21.
18. B.T. Wang, E.K. Dimitriades and C.R. Fuller, "Active control of structurally radiated noise using multiple piezoelectric actuators", *AIAA J.*, **29**, 1802-1809 (1991).
19. B. Widrow and S.D. Stearns, *Adaptive signal processing*, Prentice Hall, Englewood Cliffs, New Jersey (1985).

Farewell Scott